Available at www.sciencedirect.com

ScienceDirect

journal homepage: www.elsevier.com/locate/he

Dynamics, NO_x and flashback characteristics of confined premixed hydrogen-enriched methane flames

O. Tuncer, S. Acharya, J.H. Uhm*

Department of Mechanical Engineering, Louisiana State University, 1419B, Patrick Taylor Hall, Baton Rouge, LA 70803, USA

ARTICLE INFO

Article history:
Received 16 March 2008
Received in revised form
12 September 2008
Accepted 13 September 2008
Available online 22 November 2008

Keywords:
Spray combustion
Mixing
Forced dilution jet

ABSTRACT

The operating regime of a gas turbine combustor is highly sensitive to fuel composition changes. In particular, the addition of hydrogen, a major constituent of syngas, has a major effect on flame behavior due to the higher burning rates associated with hydrogen. A laboratory scale premixed test rig is constructed in order to study such effects. The fuel composition is incremented with increasing hydrogen starting from 100% methane. It is observed that increased RMS pressure levels and higher susceptibility to flashback occur with increasing hydrogen volume fraction. Furthermore, hydrogen enrichment can cause an abrupt change in the dominant acoustic mode. Measurements are reported of real-time heat release, emissions and flashback. Particular emphasis is put on understanding the relationship between the thermo-acoustic induced pressure oscillations and flashback.

1. Introduction

Modern premixed gas turbine combustors are usually operated near the lean blowout limit due to emission requirements [11]. Lean premixed combustion decreases the adiabatic flame temperature thus reducing the production rate of nitric oxides which is highly temperature dependent [29]. In this operating range flame holding and thermo-acoustic instability become the two most important considerations. Thermo-acoustic instability not only deteriorates the material structure of the combustor subjecting it to fatigue loading [6], but also can induce flashback into the premixing section [9]. Lean premixed natural gas combustion has been extensively studied; however, as the transition is made from natural gas to hydrogen-enriched fuels (e.g., syngas), the impact of hydrogen addition on the key performance metrics is not well understood [17]. Therefore, near lean blowout behavior of syngas needs to be explored in a detailed manner.

Thermo-acoustic oscillations occur because unsteady heat release couples positively with sound waves producing large velocity and pressure perturbations [6]. If the unsteady heat input is in phase with pressure perturbations acoustic waves gain energy and instability takes place. Strength of these oscillations is limited by non-linear effects such as fuel consumption rates, and limit cycle oscillations occur. However, these oscillations can be sufficiently strong that they can cause gas turbines to shut down or cause hardware damage. If the pressure oscillations are strong enough they can cause the flame to enter into the premixing section triggering flashback. This phenomenon is called as thermo-acoustic instability induced flame flashback.

Synthesis gas is a variable mixture of primarily hydrogen (H_2) and carbon monoxide (CO). Depending on the gasification process variables, and which solid is gasified, substantial changes in the resulting syngas composition occurs [19]. These changes in the syngas composition can significantly alter the flame behavior [20]. Therefore, the composition of the fuel impacts the turbine life and emissions [4], and characterization of the flame behavior at different fuel compositions is an important task. Furthermore, syngas combustion is

* *Corresponding author.*
E-mail address: acharya@me.lsu.edu (S. Acharya).
0360-3199/$ – see front matter © 2008 International Association for Hydrogen Energy. Published by Elsevier Ltd. All rights reserved.
doi:10.1016/j.ijhydene.2008.09.075

Nomenclature

A	Cross sectional area/Einstein coefficient for spontaneous emission
B	Einstein coefficient for stimulated absorption
C	Concentration
D	Combustor diameter
$f_{J''}$	Boltzmann fraction of the tracer species in absorbing state
g	Spectral convolution of the laser spectral distribution and the absorption transition
L	Flame height/Combustor length
M	Mach number
n_o	Number of tracer molecules
n_{tot}	Total number density
P	Pressure
Q	Rate of electronic quenching to the lower state
S	Flame speed
S_f	Fluorescence signal
T	Temperature
t	Time
U	Longitudinal velocity
V_c	Collection volume
x	Longitudinal coordinate

Greek Symbols

φ	Equivalence ratio/Fluorescence yield
ω	Frequency
α	Thermal diffusivity of reactants/Hydrogen volume fraction
η	Overall efficiency of the optical setup

Subscripts

A	Air
ad	Adiabatic
f	Flame
F	Methane fuel
in	Inlet
L	Laminar
ref	Reference

Superscripts

$\bar{}$	Time average
(.)'	Fluctuating quantity

prone to flashback due to high flame speeds associated with its hydrogen content. Under atmospheric conditions the flame speed of a stoichiometric methane air mixture is about 40 cm/s [24,26] whereas that of a hydrogen air flame is about 200 cm/s [24,25]. Therefore, hydrogen flame propagates five times faster than a methane flame under atmospheric pressure. This mismatch between flame speeds leads to flame holding problems in a gas turbine engine environment.

To achieve a desired power output from syngas, high volumetric fuel flow rates are needed due to the lower heating value of the fuel per unit volume. This causes mixing problems inside the premixer due to high injection speeds of the fuel, and affects the combustion process downstream. Another issue is the very lean burning of hydrogen-enriched mixture requires more combustion air. Resulting high volumetric flow rates then translate into higher axial speeds inside the premixer which lowers mixing time. This axial velocity also tries to push the flame away from its anchoring point (i.e. the center body in this particular case) at the dump plane which poses significant problems with respect to flame holding and can yield to a complete blow-off [2,3,15]. In this paper, we present measurements with hydrogen-enriched natural gas, and examine the role of hydrogen addition on the performance of the gas turbine combustor. By taking advantage of the single mode limit cycle oscillations, the phase resolved behavior of the unsteady processes (thermo-acoustics and flashback) can be examined.

2. Experimental setup

Fig. 1 shows a schematic of the experimental setup that includes the combustor, gas bottles, metering systems, and the instrumentation. The combustor system consists of the combustor shell, the inlet fuel and air-delivery system, and the premixing section. The combustor shell is comprised of two pieces (see Figs. 2 and 3). A 2.75" inner diameter quartz tube sits on a stainless steel flange that defines the dump plane. Quartz tube enables optical access into the main recirculation zone. Following the quartz tube there is a cylindrical stainless steel shell followed with as conical constriction section where the exhaust flow diameter drops down to 0.5". On the stainless steel shell there are ports to enable pressure transducer mounting and there is also a port to enable gas sampling. The basic design of the fuel-air premixing section represents a generic configuration with characteristic features similar to industrial gas turbine systems where the fuel is injected into the swirling cross flow and mixes within a downstream distance before reaching the dump plane. More detailed discussion about the design of this specific combustor can be found in [21–23]. Combustor is operated up to a power rating of 20 kW. Quartz tube and the stainless steel shell are cooled on the outer wall by means of forced convection air-jets during combustion.

Combustion air is fed through an eight-blade 45o-swirl vane (see Fig. 3). A correlation [1] gives the corresponding swirl number as $Sw = 0.98$. Swirl provides stabilization at the dump plane and facilitates the entrainment of fuel jets within the cross flow at the premixer.

Hydrogen H_2 and methane CH_4 gases are individually supplied from compressed tanks and mixed within a manifold prior to combustor inlet (see Fig. 1). Their flow rates are controlled by separate mass flow meters. Mass flow rates are adjusted separately in order to achieve the desired fuel composition. Air necessary for combustion is supplied from a 290 psig, 450 ACFM air compressor. Volumetric airflow rate is measured by a rotameter, and a pressure gage at the rotameter exit is used to correct the readings.

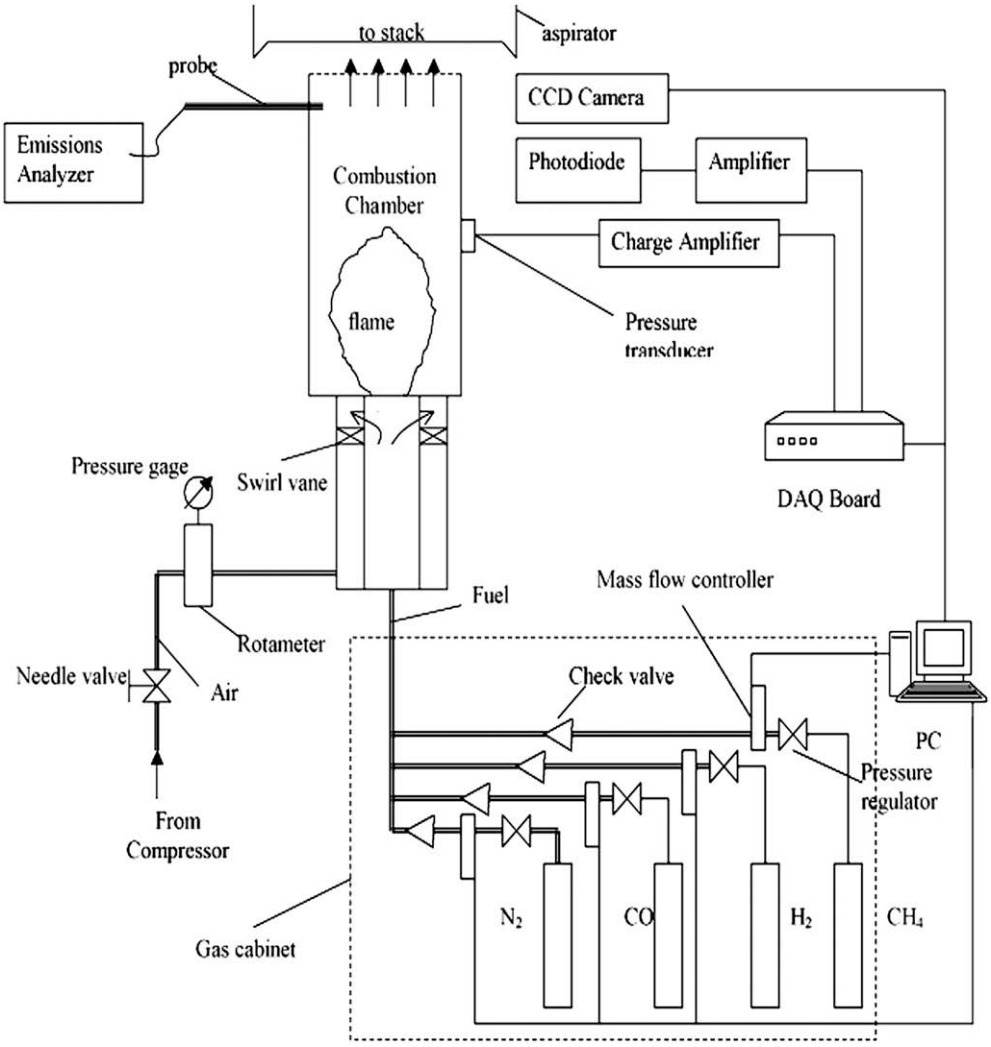

Fig. 1 – Schematic of experimental setup.

3. Results and discussion

Unlike natural gas, synthesis gas flame has a much different behavior due to different laminar flame speed (mainly due to its hydrogen constituent) and adiabatic flame temperature. Both the laminar flame speed and adiabatic flame temperature heavily depend on mixture composition. Since there are multiple fuels in a methane and hydrogen mixture (which is used as a proxy to study methane & syngas mixtures) a suitable definition of the equivalence ratio, which takes the overall stoichiometry into account, is needed. Following the assumptions made by Yu et al. [27] an equivalence ratio is defined as follows (see Eq. (1)). This equation assumes that the hydrogen in the blend is completely oxidized and the remaining oxygen is used to burn the methane content (note that the subscript "F" refers to methane). This is a reasonable assumption since the hydrogen oxidation proceeds much faster than methane oxidation.

$$\phi = \frac{C_F/\left[C_A - C_H/(C_H/C_A)_{st}\right]}{(C_F/C_A)_{st}} \quad (1)$$

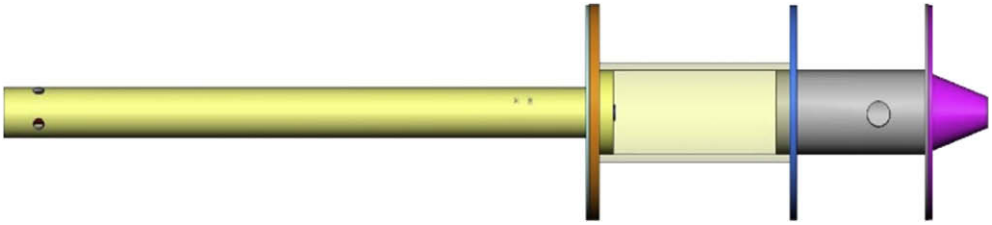

Fig. 2 – Overall view of the combustor.

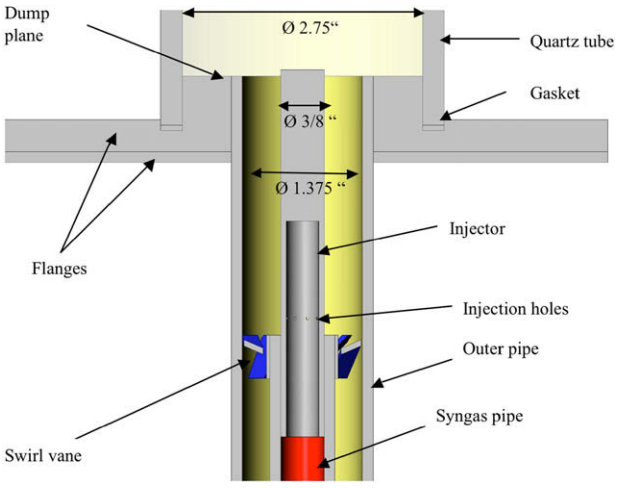

Fig. 3 – Close-up view of the fuel delivery section.

3.1. *Lean blowout (LBO) measurements*

Gas turbine engines are operated near their lean blow-off limits due to emissions considerations. Hydrogen enrichment considerably extends the lean blowout limits of the methane fuel, and evidence of this is shown in Fig. 4. These effects regarding the extension of lean blowout limits through hydrogen addition are consistent with the recent observations reported by [7,18,28]. As seen in Fig. 4, hydrogen enrichment extends the LBO limit quite extensively. It is also observed that for hydrogen-enriched methane LBO equivalence ratio is not fixed, it both depends on the extent of enrichment and on the flow rate as shown in Fig. 4. At higher flow rates higher hydrogen content was necessary to sustain the flame. Equivalence ratio at lean blowout

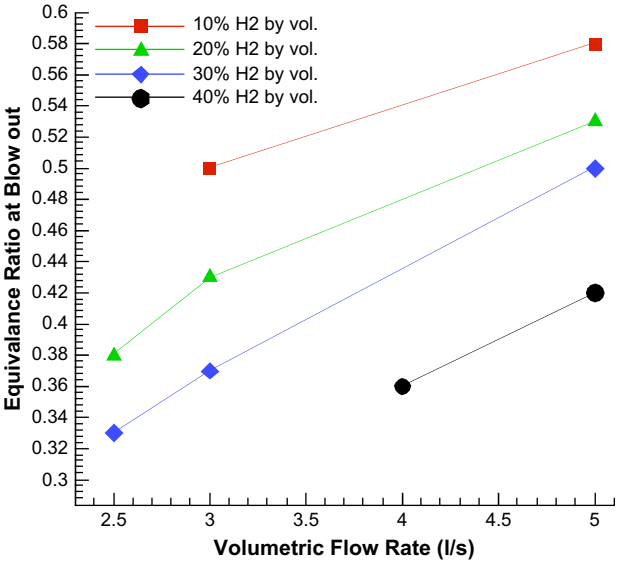

Fig. 4 – Lean blowout limits as a function of percent hydrogen volume fraction (α).

increases as the volumetric flow rate (hence fluid velocity) increases for all fuel compositions.

In flamelet combustion regime blowout occurs when the local flame speed is less than the oncoming fluid velocity everywhere in the flame. Thus the stabilization mechanism for flamelet-like combustion is based on the flame front propagation [28]. Turbulent flame speed is often expressed in terms of laminar flame speed multiplied by a function which depends both on turbulence intensity and geometry. For all conditions tested in the laboratory combustor, the geometry is fixed, so those can be factored out when correlating the blowout behavior. Assuming turbulence intensities are similar, as a first order approximation, the loading parameter can be expressed in terms of the laminar flame speed of the fuel mixture. For a two-fuel blend one can express flame speed as a sum of individual species' flame speed weighted by their mole fractions inside the fuel blend (Eq. (2)) as a first order semi-empirical approximation and agrees with experimental data. Both di Sarlia & di Benedetto [5] Kröner et al. [10] provide CH_4/H_2 laminar flame speeds. Results as per Eq. (2) are tabulated in Table 1 for a quick reference.

$$S_L = \frac{C_F}{C_F + C_H} S_{L,CH_4,\phi} + \frac{C_H}{C_F + C_H} S_{L,H_2,s} \quad (2)$$

Note that the flame speed of hydrogen is considered at stoichiometric conditions due to the same assumptions made for the definition of the equivalence ratio. Flame speed of methane on the other hand depends on the equivalence ratio as calculated from Eq. (1). Consequently, the flame speed of the mixture is calculated using the above equation. Flow speed U is the azimuthal velocity component of the cold reactants at the dump plane as per Zhang et al. [28]. Results are demonstrated in Fig. 5. This figure shows the relationship between lean blowout equivalence ratio and flamelet based loading parameter. Data for blowout is recorded in a wide range of operating conditions $2.5 \leq \dot{Q}_{air} \leq 7.1$ l/s, $0.4 \leq \phi \leq 1.3$ as well as a wide range of fuel compositions (from pure methane to 50% methane/50% hydrogen with the hydrogen concentrations indicated by the color map). As it can be seen from this figure data points are roughly correlated by a single line with a correlation coefficient of 0.69.

Chemical time scales for hydrogen and methane oxidation are quite different. Therefore considering the turbulence in practical combustors, combustion process can indeed cover a wide spectrum of Damköhler numbers. Another reactor

Table 1 – Laminar flame speeds (in m/s) of CH_4/H_2 mixtures at 1 atm.

	$\varphi = 0.7$	$\varphi = 0.8$	$\varphi = 0.9$	$\varphi = 1.0$
0% H_2 by vol.	0.20	0.27	0.33	0.40
10% H_2 by vol.	0.38	0.44	0.50	0.56
20% H_2 by vol.	0.56	0.62	0.66	0.72
30% H_2 by vol.	0.74	0.79	0.83	0.88
40% H_2 by vol.	0.92	0.96	1.00	1.04
50% H_2 by vol.	1.10	1.14	1.17	1.20

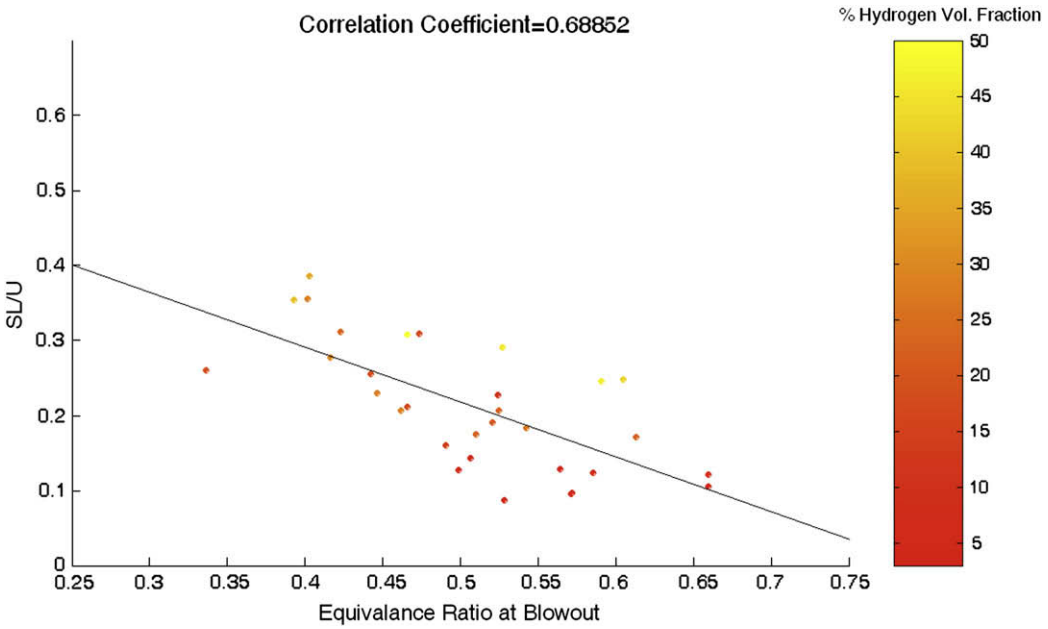

Fig. 5 – Relationship between blowout equivalence ratio and flamelet based loading parameter.

loading parameter L_2 based on a well-stirred reactor approach can be defined as well (Eq. (3)). Following the work of Hoffman et al. [8], azimuthal velocity component U_θ and combustor diameter D are used as the appropriate scaling parameters. Here α denotes the thermal diffusivity of the reactant mixture.

$$L_2 = \frac{\alpha U}{S_L^2 D} \tag{3}$$

Results for reactor based correlation are shown in Fig. 6. For this parameter L_2 however, correlation is weaker compared to the flame speed correlation. The correlation coefficient is only 0.41. Especially for low hydrogen content mixtures (shown with darker spots on the plot) one observes that there is a very large scatter in the data. This in turn points out that well-stirred reactor based loading does not offer a good explanation for methane rich mixtures. On the other hand, one can see that for hydrogen rich mixtures (indicated with lighter shades) data seems to correlate better with this loading parameter. More discussion on this issue will be provided at a later section while discussing PLIF measurement results.

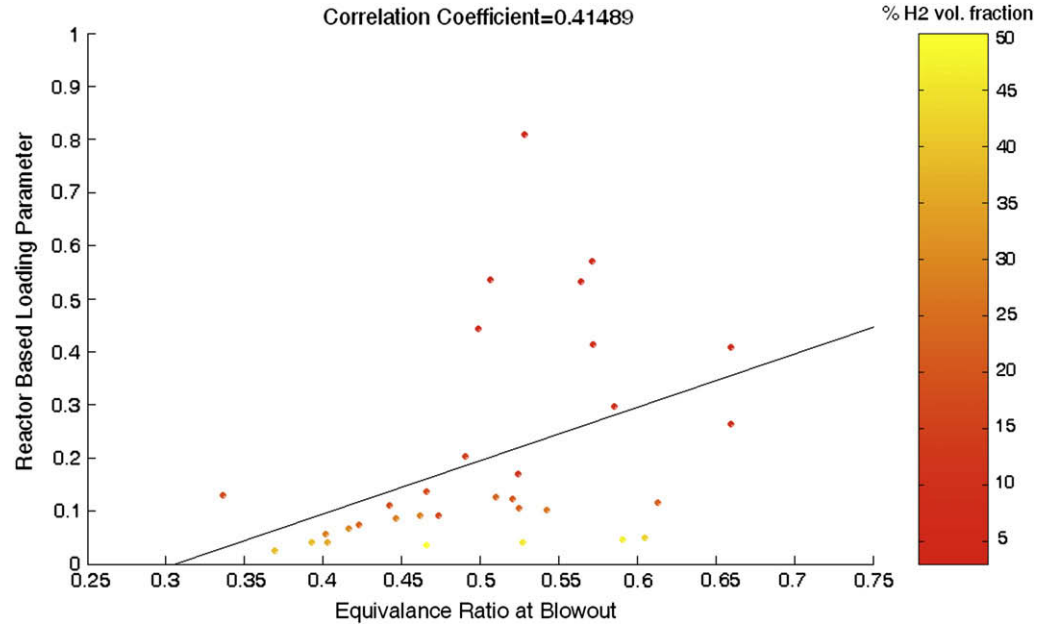

Fig. 6 – Relationship between blowout equivalence ratio and reactor based loading parameter.

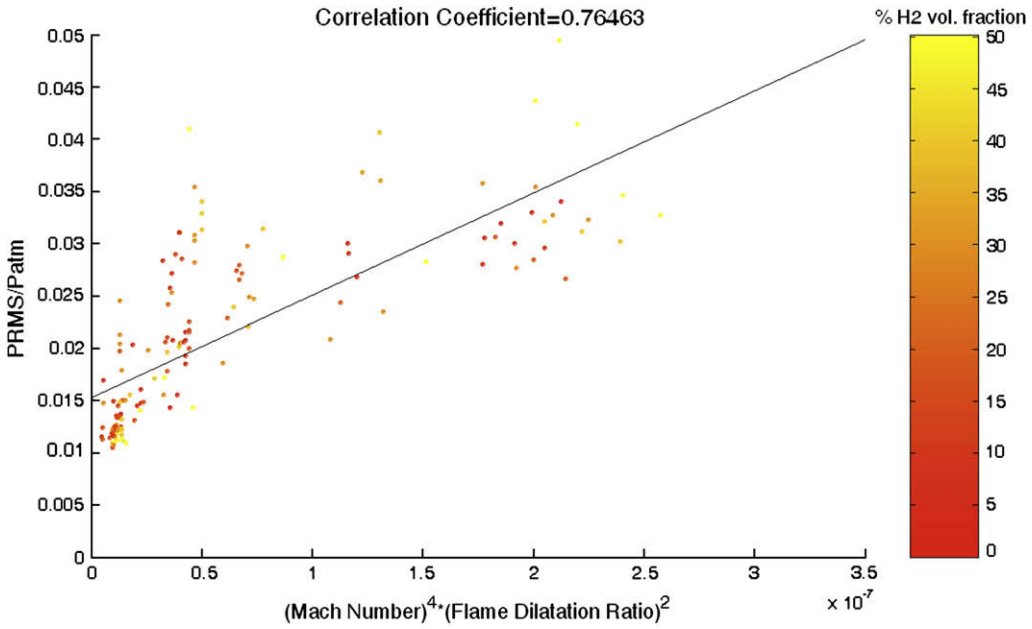

Fig. 7 – Scaling of RMS pressure level ($0.4 \leq \phi \leq 1.3$, $149 \leq \dot{Q}_{air} \leq 426$ lt/min).

3.2. *Pressure, heat release and flashback measurements*

Six Kistler 7061 water-cooled piezo-electric pressure transducers are mounted along the combustor wall, and measure dynamic pressure variations in the combustor. In order to examine the waveform of the combustion instability pressure inside the reactor is measured at several stations along the entire length of the combustor.

Fig. 7 shows the scaling of RMS pressure levels which is linked to the amplitude of the combustion generated noise. Data points shown in the scatter plot covers a wide parameter space (i.e. equivalence ratio, flow rate and mixture composition). Data points showing extinction re-ignition behavior near the lean blowout limit are typically characterized by high amplitude pressure fluctuations. These points are not shown in this plot as these belong to an entirely different regime. Combustion generated noise typically depends on Mach number and flame dilatation ratio. Flame dilatation ratio is defined as the temperature ratio of burned gases to the unburned reactants. Combustion generated noise scales with the second power of the flame dilatation ratio. For the Mach number on the other hand, combustion generated noise has a fourth power dependence. A more detailed treatment and derivations can be found in Lieuwen et al. [12,13]. Correlation coefficient of the linear trendline fitted to the scatter points is 0.76.

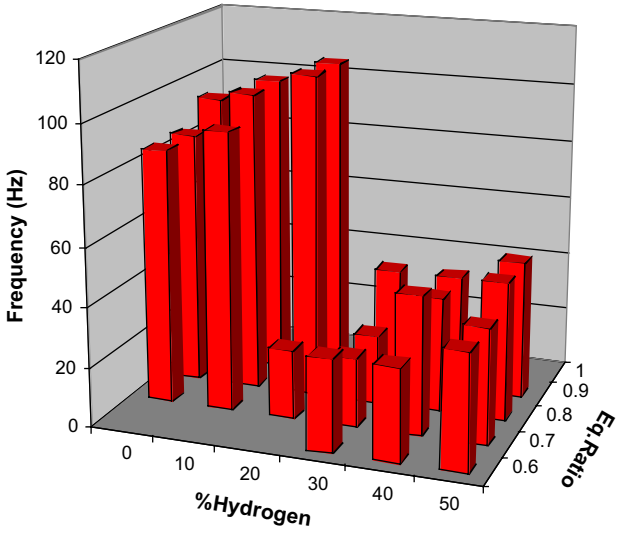

Fig. 8 – Dominant frequency (Hz) with respect to fuel composition and equivalence ratio ($\dot{Q}_{air}$ = 374 lpm).

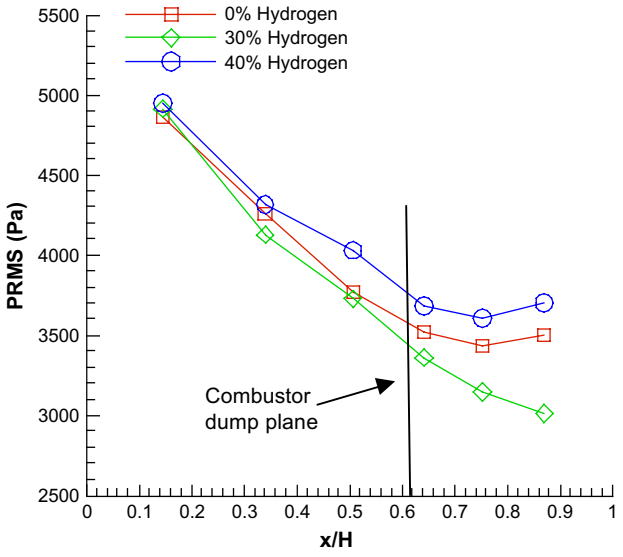

Fig. 9 – RMS pressure variation along the combustor axis.

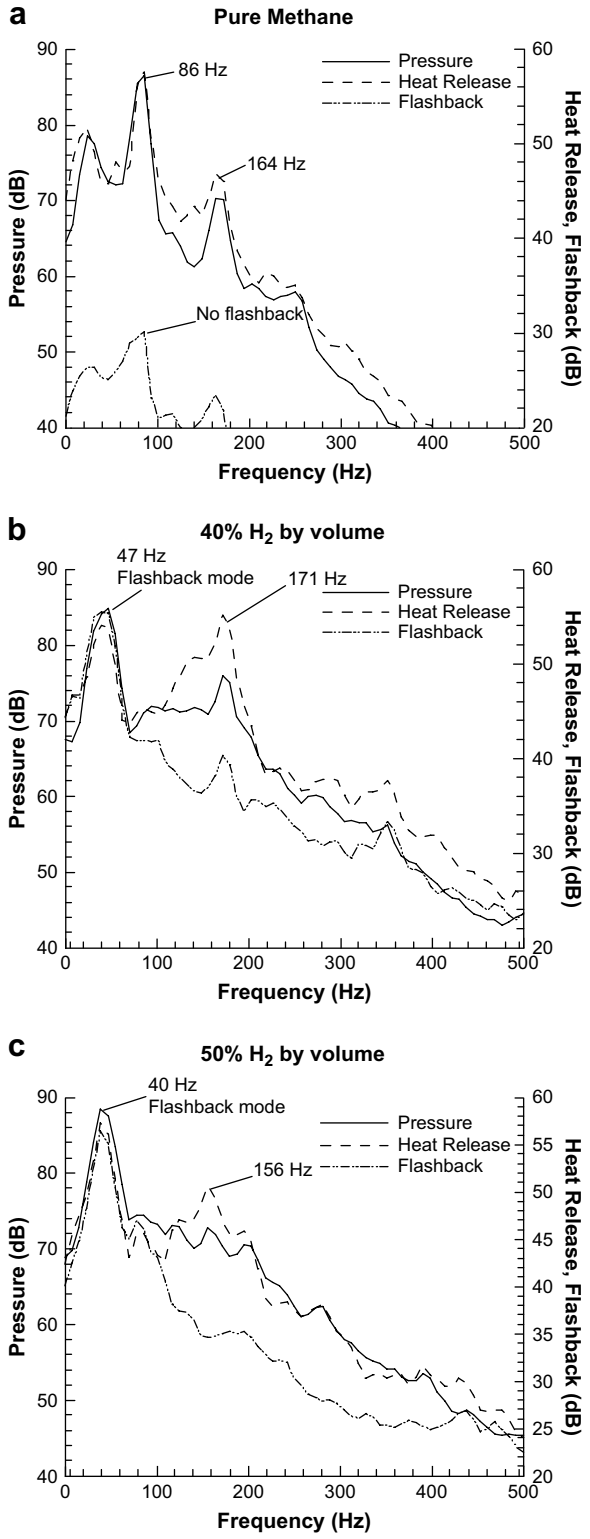

Fig. 10 – Pressure, heat release and flashback spectra ($\dot{Q}_{air}$ = 7.1 l/s, φ = 0.7).

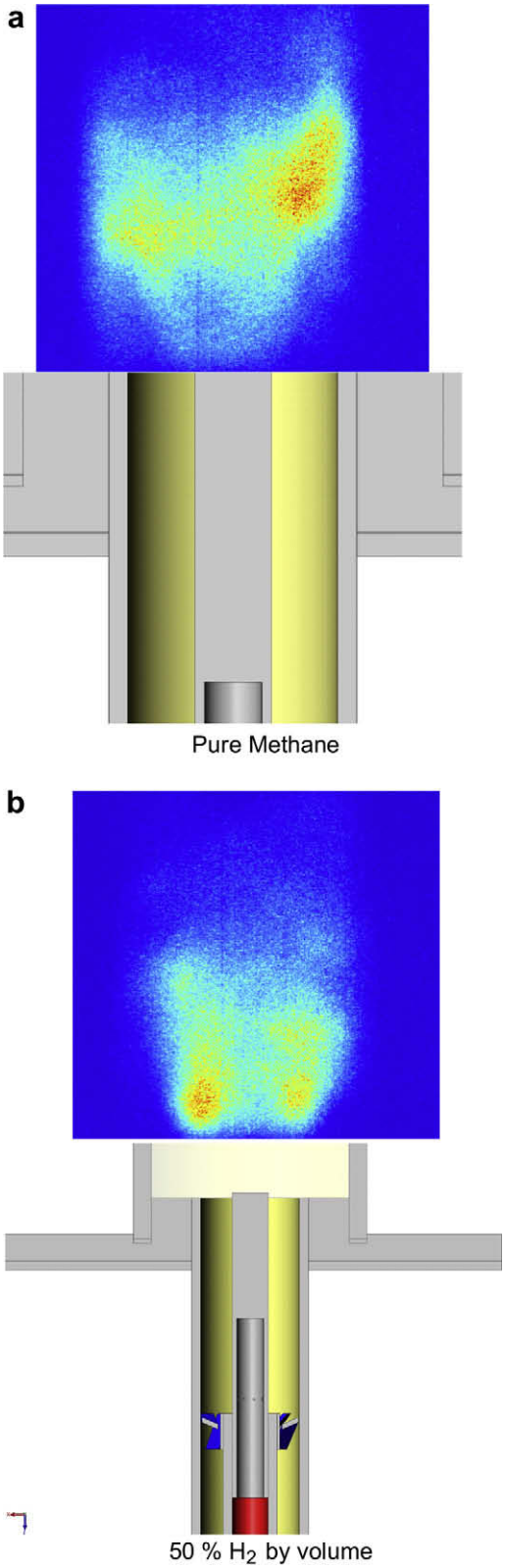

Fig. 11 – OH* Chemiluminescence Images demonstrating effect of fuel composition on the distance to the flame center of mass at a fixed flow rate and equivalence ratio ($\dot{Q}_{air}$ = 6.2 l/s, φ = 0.7).

The CH/OH radical light intensity is recorded using a silicon PIN photodiode (Melles-Griot) looking at the flame equipped with an appropriate band pass optical filter. Collected light is focused onto the sensor area by a convex lens. For CH radical

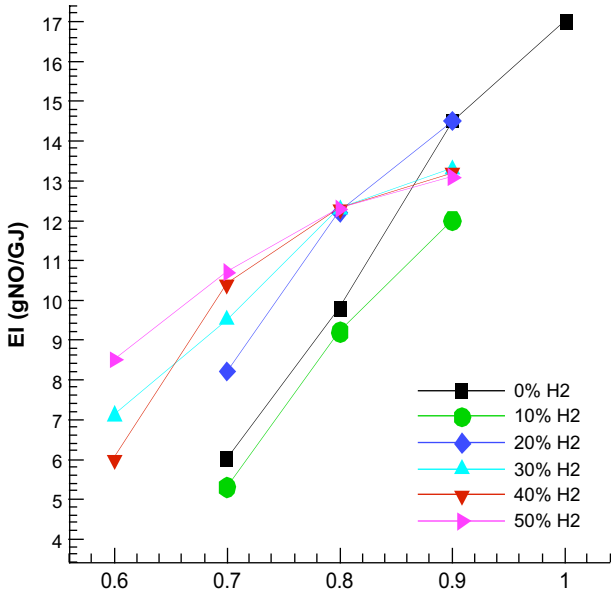

Fig. 12 – EI as a function of equivalence ratio and hydrogen volume fraction.

a filter centered at 430 nm with a 10 nm FWHM transmission width is used. Photodiode reading is taken as a measure of integral heat release fluctuations in the main reaction zone of the reactor. In order to detect flame flashback a separate photodiode is used. This photodiode sees flashback through a fiber optic cable which is mounted at the premixing section. There is no optical filter mounted with this photodiode and the fiber optic cable transmits light at the visible spectrum. Fiber optic cable is mounted 15 mm upstream of the combustor dump plane. When the flame enters inside the premixer and travels this distance, it is seen by the photodiode and the light signal is converted into voltage which is in turn recorded by the DAQ board along with the other signals.

Fig. 8 demonstrates the dominant frequency of combustion as a function of equivalence ratio and fuel composition. Two distinct regions of dominant mode, one with higher frequency (around 90 Hz), the other one with lower frequency (around 30–50 Hz) can be easily identified. This transition occurs around 20–25% hydrogen content, and as will be discussed later, represents conditions where flashback is initiated. The flashback is associated with periodic low frequency fluctuations, with the flame flashing back and recovering, and these fluctuations are at the observed pressure oscillation frequency. This implies that the periodic flashback is coupling with the air-delivery-chamber/combustor acoustics with a positive feedback.

Fig. 9 shows the longitudinal distribution of the pressure RMS for no-hydrogen and with-hydrogen. In Fig. 9, x is the distance measured from the combustor inlet, and H is the overall length of the combustor. Dump plane is located at $x/H = 0.6$. In all cases RMS pressure decays with the streamwise distance going from acoustically closed inlet to the acoustically open outlet. RMS pressure amplitudes increase with increasing hydrogen content. This effect is more pronounced towards the combustor exit. Although there is a sudden drop in the dominant frequency (see Fig. 8) RMS pressure waveform does not experience a substantial change as seen in Fig. 9.

Fig. 10 shows the spectra of pressure, heat release and flashback signals on a logarithmic scale. The frequency shift associated with the hydrogen addition (Fig. 8) is observed in more detail in Fig. 10. For pure methane, the flashback signal amplitude is low, and is at the noise level associated with the indirect flame radiation "(i.e. indirect optical reflections from the combustion chamber into the location where the fiber optic cable is mounted). At 40–50% hydrogen (Fig. 10b,c) the flashback signal in the 40–47 Hz range is clearly evident. The flashback activity and change in the dominant frequency in the pressure oscillations accompany one another, and are both at the same frequency. This implies that as the flame

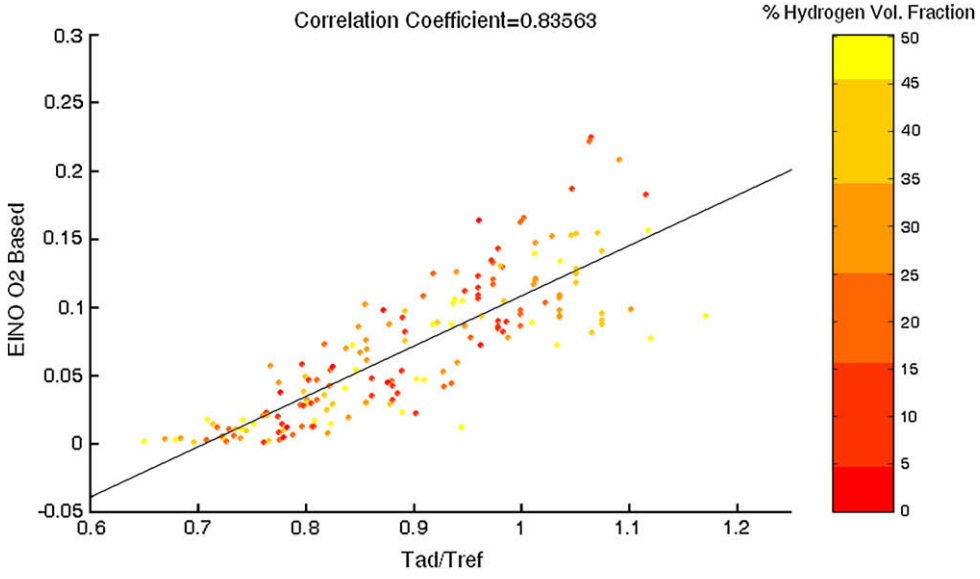

Fig. 13 – Relationship between adiabatic flame temperature and emissions index over a wide range of load conditions ($0.4 < \phi < 1.3$, $0.5 < \dot{Q}_{air} < 7.1$ lt/s).

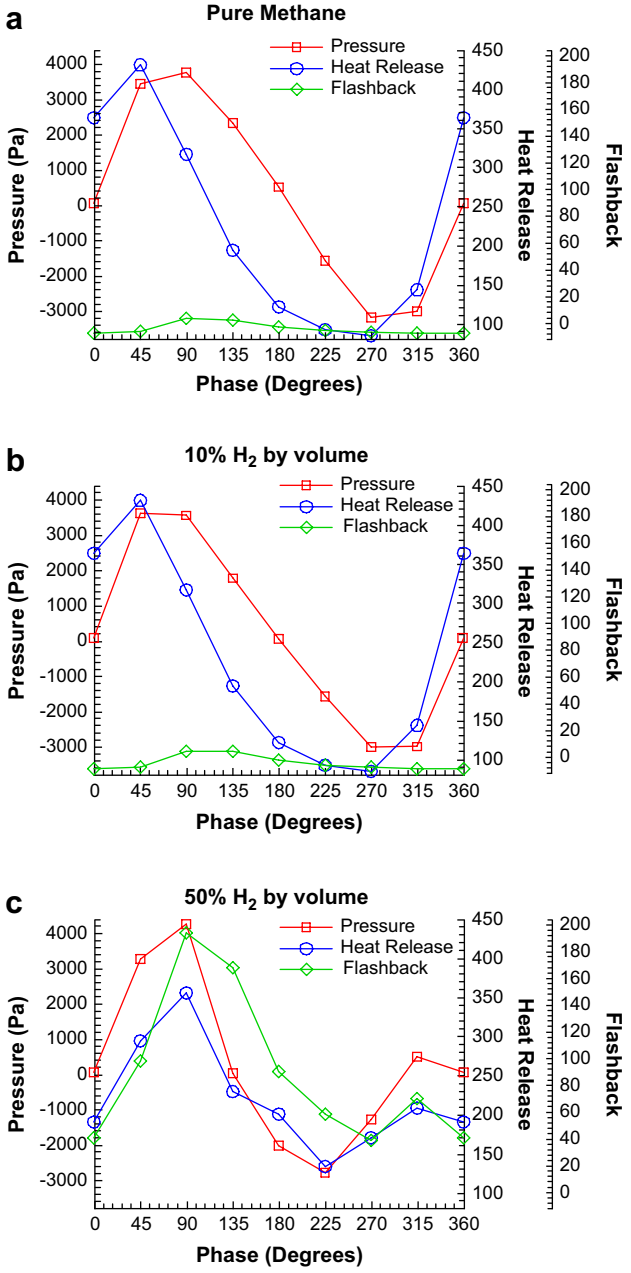

Fig. 14 – Phase averaged pressure, heat release and flashback signals.

moves up and down inside the premixer and generates heat release fluctuations at the flashback frequency, the resulting heat release dynamics couples with an acoustic mode of the combustor system exciting this mode. This behavior is phase resolved in a latter section of the article.

Another way through which fuel composition affects the feedback route between heat release and pressure fluctuations within the thermo-acoustic loop is the change that occurs when the flame center of mass is changed due to change in flame speed. As the flame speed increases with the addition of hydrogen the flame becomes shorter and the distance to the flame center of mass (center of heat release) decreases. This yields a reduced convective time for the equivalence ratio perturbations which can cause a stable combustor to become unstable and vice versa [12,13]. Fig. 11 shows the change in flame center of mass with varying fuel composition while keeping the inflow velocity constant to factor out the aerodynamic effects. These are time averaged two dimensional hydroxyl chemiluminescence images captured with an intensified CCD camera equipped with an appropriate band pass filter. For each image, the CCD array is gated for 10 μs and a total of 400 images are recorded for averaging. One can notice the change in the location between two flow conditions tested. With 50% methane and 50% hydrogen, most of the heat release takes place in spatial locations closer to the dump plane. Inlet section, dump plane and the location fuel injector are also schematically shown in this figure.

3.3. *Emissions measurements*

Nitric oxide emission measurements have been performed using a chemiluminescence analyzer. A water-cooled probe is placed at the combustor exit. Exhaust gases are sucked at the center. Keeping the other variables constant (i.e. equivalence ratio, volumetric flow rate) and increasing the hydrogen volume fraction of the fuel results in increased nitric oxide emissions index values (see Fig. 12). In Fig. 12 emissions are reported in gNO/GJ units, as the mass of nitric oxide generated per a given amount of heat input due to combustion. On the other hand hydrogen enrichment enables the sustainment of combustion at much leaner equivalence ratios than those are ever possible with methane. Premixed lean combustion has long been utilized as an industry standard technique to reduce nitric oxide emissions. Even though hydrogen addition increases NO_x emissions at a fixed equivalence ratio the overall emissions still can be reduced by burning leaner mixtures of methane and hydrogen blend, which were impossible for the pure methane case. This will reduce the adiabatic flame temperature reducing the thermal and other contribution to the total NO_x emissions index. Thus it becomes possible to burn a CH_4/H_2 fuel blend (although under leaner conditions) without increasing nitric oxide emissions over the pure CH_4 baseline condition.

Fig. 13 shows the correlation between adiabatic flame temperature and nitric oxide emissions index (EINO) over a wide parameter space including fuel variability effects. Points on the scatter plot are color coded according to the binary fuel mixture composition. Note that for the flow conditions tested the residence time changes by almost a factor of three. Residence time is one of the determining parameters for the equilibrium concentration of species. However, as seen in Fig. 13, the correlation of EINO with the adiabatic flame temperature is quite good, with a correlation coefficient of nearly 0.8, and one can therefore argue that the residence times are longer than the NO-formation timescales, and therefore the effects of residence time play a relatively smaller role. The increase in the nitric oxide emissions index with increasing hydrogen is potentially linked to the associated increased concentration of the hydroxyl (OH) radicals within the radical pool. Higher hydroxyl concentrations can increase the forward reaction rates in the nitric oxide formation mechanism involving the OH radical. However, as Fig. 13 suggests the main scaling parameter is the adiabatic flame temperature. Yet, this does not mean that residence times are insignificant. In fact, most of the data scatter shown in Fig. 13 is due to the effect of varying

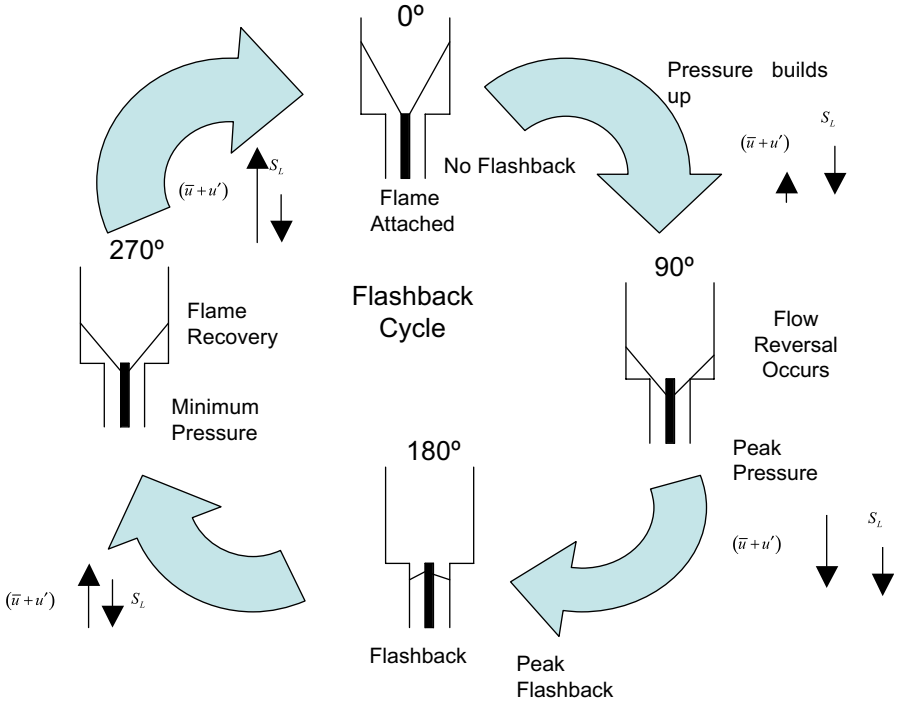

Fig. 15 – An illustration showing the cycle of events regarding flashback.

residence time. Much shorter residence times of course favor lower nitric oxide emissions due to chemical inequilibrium. If all residence times on the other hand are longer than the formation time scale of NO emissions, then emissions levels reach closer to equilibrium values. It can therefore be concluded that the extended Zeldovich mechanism (thermal NO_x) is the dominating pathway to NO formation in this case. Residence time, albeit it has a smaller impact, should be responsible from the scatter in the data points.

Fig. 14 demonstrates the phase averaged behavior of pressure, heat release and flashback signals. In view of the instability, pressure and heat release signals are nearly in phase with each other resulting in a positive Rayleigh index. In Fig. 14a,b corresponding respectively to pure methane, and 10% hydrogen by volume, the flashback signal is flat suggesting no flashback activity at these conditions. However, in Fig. 14c, the amplitude of the flashback signal shows a significant peak at the 90-degree phase instance with respect to the pressure instability cycle. Consequently flashback signal reaches its maximum value when the pressure is also at a maximum indicating the inter-relationship between the pressure dynamics and flashback. These observations support the earlier conclusions based on Fig. 10. (i.e. no flashback with pure methane and flashback with 50% H_2/50% CH_4 mixture).

Fig. 15 depicts the cycle of events leading to periodic flame flashback. Vertical arrows pointing upwards and downwards indicate total flow velocity ($U+u'$) and flame speed (S_L) respectively. The flame speed always points towards the reactant-side of the flame front. As the pressure builds up in the combustor during the pressure-oscillation cycle, it retards the flow in the premixed fuel–air delivery section; conversely, as the pressure levels reduce in the combustor, the velocities exiting the combustor section reduce. As the cartoon in Fig. 15 illustrates, the attached wedge shaped flame moves upstream due to a flow reversal shortly following pressure buildup (see figure corresponding to the 90°phase). Whenever the flame is detached from the injector tip the flame anchoring point (tip of the wedge shaped flame) moves with a velocity which is the sum of the flame speed and fluid velocity. As seen from the figure, at the mid-cycle (180°phase), the flame is entirely inside the premixer. As the cycle progresses, the pressure inside the combustor decreases and the total fluid velocity attains a positive value that exceeds the flame speed (which always points towards the reactant's side flame front), the flame recovers its shape and re-attaches to the center body tip (0°phase). For a more elaborate discussion of this phenomenon (including a theoretical background) please refer to [22,23] wherein these flame attachment and flow reversal issues are treated.

4. Concluding remarks

In this paper hydrogen-enriched confined methane combustion is studied in a laboratory scale premixed combustor. Correlating parameters for lean blowout (LBO), pressure amplitudes and emissions are examined. Two loading parameters are examined to correlate the lean blowout results: one based on a flamelet approach the other based on a well-stirred reactor approach. The flamelet based loading parameter correlates better with the blowout data. Nitric oxide emissions (EINO) scales mainly with the adiabatic flame temperature. Although hydrogen enrichment increases EINO, it also enables very lean combustion. By taking advantage of the lower LBO associated with hydrogen, the combustor can be operated under very lean conditions with low flame temperature and thus favorably impact thermal nitric oxide

emissions. Combustion noise scales roughly with the Mach number and flame dilatation ratio.

At higher hydrogen concentrations, flashback is observed and appears to trigger a shift in the pressure oscillation mode to lower frequencies. From the OH chemiluminescence, it is seen that hydrogen enrichment shifts the flame center of mass more towards the dump plane as the burning velocity is increased with hydrogen addition. It is shown that there is a close link between the pressure cycle, the periodic flashback behavior, and the NO emission.

Acknowledgments

This work would not be possible without the financial support obtained from Louisiana Board of Regents Clean Power and Energy Research Consortium (CPERC). Authors would like to express their gratitude for this support. The help and support received from Dr. Jong Ho-Uhm and Mr. Jeffrey Wilbanks during the experimental work is also gratefully acknowledged.

REFERENCES

[1] Beer JM, Chigier NA. Combustion aerodynamics. London, United Kingdom: Applied Science Publishers; 1972.
[2] Calvetti S, Carrai L, Cecchini D. Esecuzione di Prove di Co-Combustione di Gas Naturale e Syngas da Biomassa su un Combustore DLN per Turbina-Gas. Technical report, Enel Produzione, Pisa, Italy, ENELP/RIC/RT/-2001/258/0-IT + RT. RIC.PI; 2001.
[3] Calvetti S, Carrai, L, Cecchini D. Progettazione di un Combustore DLN Prototipo per TG per la Co-Combustione di Gas Naturale e Syngas da Biomassa. Technical report, Enel Produzione, Pisa, Italy, ENELP/RIC/RT/-2001/146/0-IT + RT. RIC.PI; 2001.
[4] Cowell L, Etheridge C, Smith K. Ten years of industrial gas turbine operating experiences; 2002. ASME paper No: GT-2002-30280.
[5] Di Sarli V, Di Benedetto A. Laminar burning velocity of hydrogen-methane/air premixed flames. International Journal of Hydrogen Energy 2007;32:637–46.
[6] Dowling AP. The calculation of thermoacoustic oscillations. Journal of Sound and Vibration 1995;180:557–81.
[7] Guo H, Smalwood GJ, Liu F, Ju Y, Gulder OL. The effect of hydrogen addition on flammability limit and NO_x emission in ultra-lean counterflow CH_4/air premixed flames. Proceedings of the Combustion Institute 2005;30:303–11.
[8] Hoffman S, Habisreuther P, Lenze B. Development and assesment of correlations for predicting stability limits of swirling flames. Chemical Engineering and Processing 1994; 33:393–400.
[9] Kiesewetter F, Hirsch C, Fritz M, Kroner M, Sattelmayer T. Two-dimensional flashback simulation in strongly swirling flows; 2003. ASME paper No: GT2003-38395.
[10] Kröner M, Fritz J, Sattelmayer T. Journal of Engineering for Gas Turbines and Power 2003;125:693–700.
[11] Lawn CJ. Interaction of the acoustic properties of a combustion chamber with those of premixture supply. Journal of Sound and Vibration 1999;224:785–808.
[12] Lieuwen T, McDonell V, Petersen E, Santavicca, D. Fuel flexibility influences on premixed combustor blowout, flashback, autoignition and stability; 2006. ASME paper No: GT2006-90770.
[13] Lieuwen T, Mohan S, Rajaram R, Preetham. Acoustic radiation from weakly wrinkled premixed flames. Combustion and Flame 2006;144:360–9.
[15] Mariotti M, Tanzini G, Faleni M, Castellano L. Sperimentazione di Fiamme di Idrogeno a Pressione Atmosferica in un Combustore per Turbogas con Iniezione di Inerti. Technical report, Enel Produzione, Pisa, Italy, ENELP/RIC/RT/-2002/0063; 2002.
[17] Morris JD, Symonds RA, Ballard FL, Banti A. Combustion aspects of application of hydrogen and natural gas fuel mixtures to MS9001E DLN-1 gas turbines at Elsa plant. The Netherlands: Terneuzen; 1998. ASME paper No: GT98-35.
[18] Schefer RW. Reduced turbine emissions using hydrogen enriched fuels. In: Proceedings of the 2002 U.S. DOE hydrogen program review, NREL/CP; 2002.
[19] Smoot LD, Smith PJ. Coal combustion and gasification. New York: Plenum Press; 1985.
[20] Tomzcak H, Benelli G, Carrai L, Cecchini D. Investigation of a gas turbine combustion system fired with mixtures of natural gas and hydrogen. IFRF Combustion Journal 2002. Article number: 200207.
[21] Tuncer O. Active control of spray combustion. PhD dissertation, Louisiana State University, Baton Rouge, LA; 2006.
[22] Tuncer O, Acharya S, Uhm JH. Effects of hydrogen enrichment on confined methane flame behaviour. In: Proceedings of ASME power 2006, Atlanta, Georgia; 2006. ASME paper No: PWR2006-88079.
[23] Tuncer O, Acharya S, Uhm JH. Hydrogen enriched confined methane flame behavior and flashback modeling. In: Fourty-fourth AIAA aerospace sciences meeting and exhibit, Reno, Nevada; 2006. AIAA paper No: AIAA 2006-754.
[24] Vagelopoulos CN, Egolfopoulos FN. Direct experimental determination of laminar flame speeds. In: Twenty-seventh symposium (international) on combustion; 1998. p. 513.
[25] Vagelopoulos CN, Egolfopoulos FN, Law CK. Further considerations on the determination of laminar flame speeds with the counterflow twin-flame technique. In: Twenty-fifth symposium (international) on combustion; 1994. p. 1341. Egolfopoulos, F.N.
[26] Van Maaren A, Thung DS, deGoey LPH. Measurement of flame temperature and adiabatic burning velocity of methane/air mixtures. Combustion Science and Technology 1994;96:327–44.
[27] Yu G, Law CK, Wu CK. Laminar flame speeds of hydrocarbon plus air mixtures with hydrogen addition. Combustion and Flame 1986;63:339–47.
[28] Zhang Q, Noble DR, Meyers A, Xu K, Lieuwen T. Characterization of fuel composition effects in H_2/CO/CH_4 mixtures upon lean blowout. ASME Paper No: GT2005-68907. Journal of Engineering for Gas Turbines and Power 2007;129: 688–94.
[29] Zimont VL. The theory of turbulent combustion at high Reynolds numbers. Combustion Explosions and Shock Waves 1979;15:305–11.